PROCEEDINGS OF SCIENCE
ONLINE ICRC 2021 THE ASTROPARTICLE PHYSICS CONFERENCE Berlin | Germany
37th International Cosmic Ray Conference 12–23 July 2021

Solar Modulation During the Descending Phase of Solar Cycle 24 Observed with CALET on the International Space Station

Shoko Miyake* **on behalf of the CALET Collaboration**
(a complete list of authors can be found at the end of the proceedings)

National Institute of Technology (KOSEN), Ibaraki College,
866 Nakane, Hitachinaka, Ibaraki, Japan
E-mail: `miyakesk@ee.ibaraki-ct.ac.jp`

The CALorimetric Electron Telescope (CALET) installed on the International Space Station has multiple event trigger modes for measuring cosmic-ray (CR) particles and gamma rays, and the observations of the low-energy CRs have been successfully performed by a Low-Energy Electron (LEE) shower trigger mode that is active only at high geomagnetic latitude. Here we have analyzed the low-energy electrons and protons to investigate the solar modulation during the descending phase of the solar cycle 24. We have confirmed that the flux of the low-energy electrons measured by CALET during the solar minimum has reached its maximum, which is comparable to or exceeding the maximum flux observed with PAMELA in the previous solar minimum period. We have also found count rates of electrons and protons at the same average rigidity showing a clear charge sign dependence as expected from the drift model of the solar modulation.

37th International Cosmic Ray Conference (ICRC 2021)
July 12th – 23rd, 2021
Online – Berlin, Germany

---

*Presenter

© Copyright owned by the author(s) under the terms of the Creative Commons
Attribution-NonCommercial-NoDerivatives 4.0 International License (CC BY-NC-ND 4.0).

PoS(ICRC2021)1270

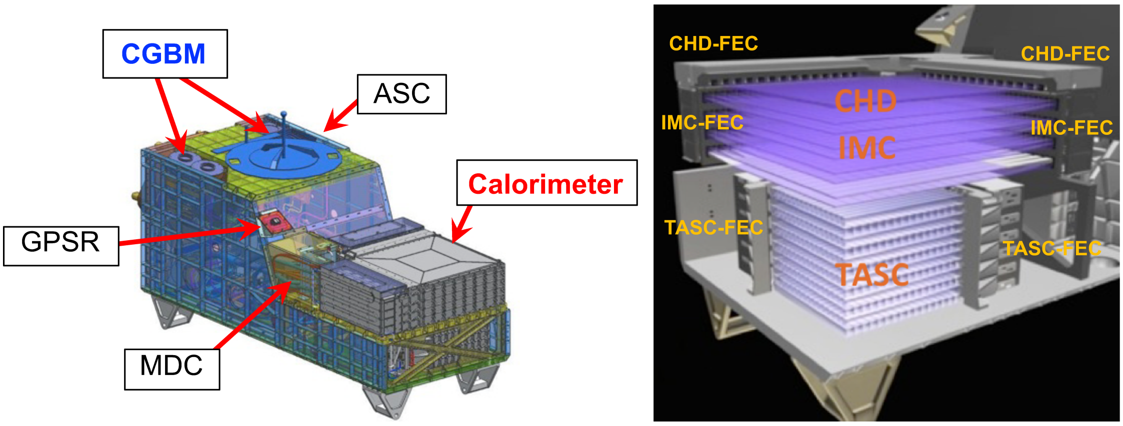

Figure 1: (Left panel) CALET instrument package showing the calorimeter, the CALET gamma-ray burst monitor (CGBM), the mission data controller (MDC), the GPS receiver (GPSR), and the advanced stellar compass (ASC). (Right panel) CALET calorimeter, which consists of a charge detector (CHD), an imaging calorimeter (IMC), and a total absorption calorimeter (TASC). The resulting output of each detector is sent to the front-end circuit (FEC).

1. Introduction

The CALorimetric Electron Telescope (CALET) is a Japanese-Italian-US international mission for precise measurements of cosmic-ray (CR) electrons (electrons + positrons) from 1 GeV to 20 TeV, gamma rays from a few GeV to 10 TeV, and nuclei with $Z = 1$ to 40 from a few 10 GeV up to ~1 PeV. The instrument was installed on the Japanese Experiment Module-Exposed Facility of the International Space Station (ISS) in August 2015, and since the beginning of operation in October 2015, continuous observations have been accomplished without any serious problem at present. Many of science goals of CALET including the investigation of possible nearby CR sources and dark matter signatures by the high-precision measurement of electron spectrum have been performed by a high-energy (HE) shower trigger mode for measuring high-energy electrons with energies above 10 GeV and the other high-energy shower events [1–4]. In addition to the HE shower trigger mode, CALET has a low-energy electron (LEE) shower trigger mode working at high geomagnetic latitudes that can measure the low-energy CR electrons in the energy region from 1 GeV to 10 GeV [5, 6]. In this study, we analyze flight data obtained by the LEE shower trigger mode from October 13, 2015 to September 30, 2020.

2. CALET Instrument

CALET has a field-of-view of ~ 45° from the zenith and an effective geometrical factor of ~ 1040 cm^2sr for high-energy electrons. The instrument of CALET consists of the main calorimeter and the CALET gamma-ray burst monitor (CGBM) subsystems as shown in a left panel of Figure 1. Details of the main calorimeter is shown in the right panel of Figure 1, which consists of a charge detector (CHD) for identifying the charge of an incident particle, an imaging calorimeter (IMC) for reconstructing the track of an incident particle and for imaging an early shower profile with a fine resolution, and a total absorption colorimeter (TASC) for absorbing the entire energies of

PoS(ICRC2021)1270

electromagnetic shower particles and for distinguishing electrons from hadrons using differences of those shower developments. The CHD is composed of two crossed layers of 14 plastic scintillator paddles with dimensions of 450 mm long × 32 mm wide × 10 mm thick. The IMC is composed of eight x-y layers of 448 mm long × 1 mm square cross section scintillating fibers (SciFi) interleaved with tungsten plates. The first five tungsten plates have 0.2 radiation length (X_0) in thickness and the last two plates have 1.0 X_0. The total thickness of the IMC is equivalent to 3 X_0. The TASC consists of twelve crossed layers of 16 lead tungstate (PWO) logs with 326 mm long × 19 mm wide × 20 mm tall, and its total thickness corresponds to 27 X_0. The thick calorimeter with 30 X_0, which is equivalent to ~ 1.3 proton interaction lengths, allows it to completely absorbs the electron shower energy even in the TeV energy range.

3. Data Analysis

We analyze flight data obtained by the LEE shower trigger mode during 1815 days from October 13, 2015 to September 30, 2020. In order to obtain the low-energy particle events efficiently, the LEE shower trigger mode is active only at high geomagnetic-latitudes where the maximum cutoff rigidity is about 5.0 GV. It means that the LEE shower trigger mode works ~ 2 times for ~ 90 sec in one orbit of ISS. We obtain a total observational live time of about 670 hours and about 79 million events of low-energy electron and proton candidates. By sorting these events and accurately subtracting the background contamination, we obtain the flux of low-energy electrons and proton count rates at the same average rigidity. The procedure to analyze the low-energy electrons and protons obtained by LEE shower trigger mode is as follows.

3.1 Monte Carlo Data

A Monte Carlo (MC) data is used to simulate physical processes and detector signals for the event selection and the energy reconstruction. The MC event samples consist of downgoing electrons and protons produced isotropically on the surface of a sphere with a radius of 78 cm which totally encloses the instrument. The interactions of secondary particle generated in the detector are treated by the simulation package EPICS [7] (EPICS 9.20 and COSMOS 8.00) and the hadron interaction is calculated by using the DPMJET-III model.

3.2 Event Selections and Energy Reconstruction

In order to minimize and accurately subtract proton contamination in the sample of electron candidates, we apply the following event selection criteria for getting the electron flux: (1) an off-line trigger condition on the energy threshold of lower two layers of IMC and TASC top layer, (2) a track quality cut based on the tracking method using the Kalman filter to ensure reconstruction accuracy, (3) a geometrical condition in which the reconstructed track traverse the instrument from the CHD top layer to the TASC bottom layer, (4) a charge selection using the CHD, (5) an energy deposit at the IMC bottom layer, (6) an energy concentration at the IMC bottom layer, and (7) a lateral shower development at the TASC top layer. These criteria are almost identical to that for the event selections of high-energy electrons obtained by the HE trigger mode [1], except that we just use TASC top layer and IMC bottom layer to prevent proton contamination, since the low-energy electrons cannot penetrate all layers of the TASC. The combined efficiency of these selections for

PoS(ICRC2021)1270

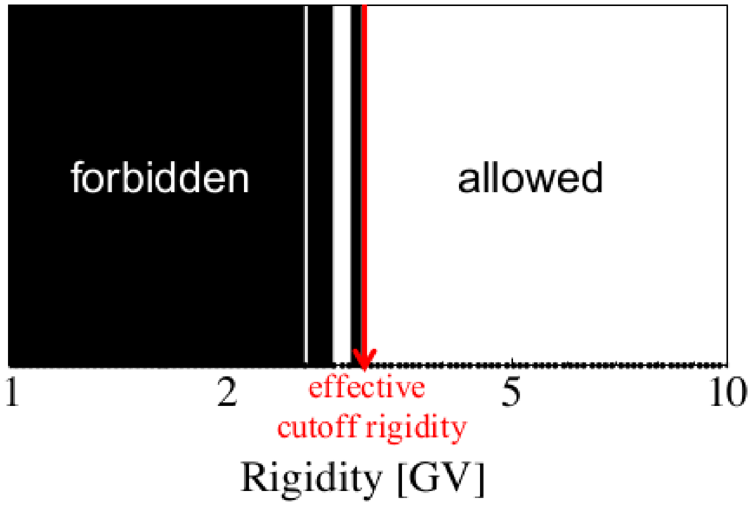

Figure 2: Example of the rigidity region that is forbidden or allowed to be detected by CALET in the geomagnetic field. An effective cutoff rigidity is defined as the lowest rigidity above which no penumbra structure appears.

the low-energy electrons is over 70% in the energy region above 2 GeV. We also evaluate an energy correction function using the electron MC data after the event selections to reconstruct the true energy of the low-energy electrons. The observed energy of the low-energy electron is defined as the sum of the energy deposit in the IMC and top three layers of the TASC to prevent adding the noise at lower layers of the TASC where the low-energy electrons cannot penetrate. The correction function is evaluated by the average ratio of the true energy to the observed energy.

In addition to the flux of low-energy electrons, we also analyze the count rates of electrons and protons that have the same average rigidity to investigate the charge-sign dependence of the solar modulation. In this analysis, due to the poor energy resolution for low-energy protons, we estimate the average rigidity of MC events that passed event selections instead of the strict energy reconstruction for each observed event. We thus obtained the average rigidity of $\sim$ 3.8 GV for the electron count rate. In order to compare the count rate of protons that has the same average rigidity as electrons, we adjusted the average rigidity of protons by applying the event selection about an energy deposit at all layers of the TASC. For the analysis of protons, we use the same event selections with that of electrons, except the energy deposit and energy concentration at the IMC bottom layer. This is because that these event selection are to prevent the proton contamination in the analysis of the electrons.

3.3 Geomagnetic Cutoff Rigidity

In order to get the flux that is not affected by the geomagnetic cutoff variation, we select events that have rigidities much higher than the geomagnetic cutoff rigidity. In the calculation of the count rates of electrons and protons, we select events that measured in the region where the cutoff rigidity is below 1.2 GV. As a reference value of the cutoff rigidity, we use the effective cutoff rigidity calculated by reconstructing particle trajectories in the magnetosphere [8], implementing a realistic description of the geomagnetic field based on the IGRF-13 and TS05 empirical models [9]. Whether

PoS(ICRC2021)1270

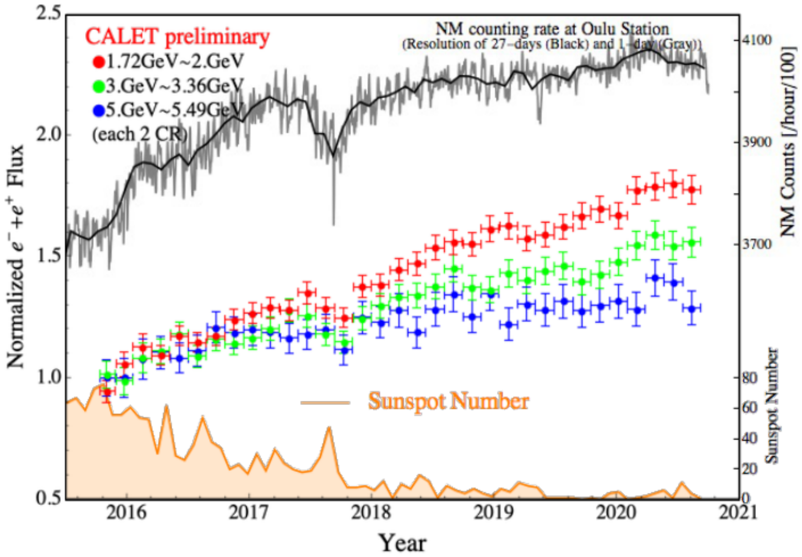

Figure 3: Time profile of the normalized flux of the low-energy electrons from October 2015 to September 2020. The fluxes in each energy are normalized with a flux during the first Carrington rotation.

or not a particle can reach CALET depends on not only the particle's rigidity but also its incident direction. In this calculation, we use the incident direction of each particle along a trajectory reconstructed by the tracking method using the Kalman filter. We then define the effective cutoff rigidity as the lowest rigidity of the allowed region above which no penumbra structure appear, as shown in Figure 2.

4. Flux of the Low-Energy Electrons

The differential flux $\Phi(E)$ between E and $E+\Delta E$ (GeV) is given by the following formula,

$$\Phi(E) = \frac{N(E)}{\Delta E \cdot \varepsilon(E) \cdot S\Omega \cdot T_L}, \tag{1}$$

where $\Phi(E)$ is expressed in $\mathrm{m^{-2}sr^{-1}sec^{-1}GeV^{-1}}$, $N(E)$ is the number of low-energy candidates in each energy bin, $\varepsilon(E)$ is the electron efficiency in each energy bin, $S\Omega\ (\mathrm{m^2sr})$ is the geometrical acceptance, and T_L (sec) is the observation time. Figure 3 shows the time profile of the average electron flux in every two Carrington rotations at three different energies since the beginning of the observation. Each flux in this plot is normalized to the flux in the first Carrington rotation. Black and gray curves show the count rate of a neutron monitor at Oulu Station (in Sodankyla Geophysical Observatory of the University of Oulu), while the orange curve displays the monthly mean sunspot number. It is seen that the solar cycle 24 is terminated in Dec. 2019 according to the Solar Cycle 25 Prediction Panel, but the electron flux in 1-10 GeV has continuously increased until about half a year after beginning the new solar cycle. The maximum flux during the current solar minimum period is comparable to or exceeding the maximum flux observed with PAMELA[10] in the previous solar minimum period.

PoS(ICRC2021)1270

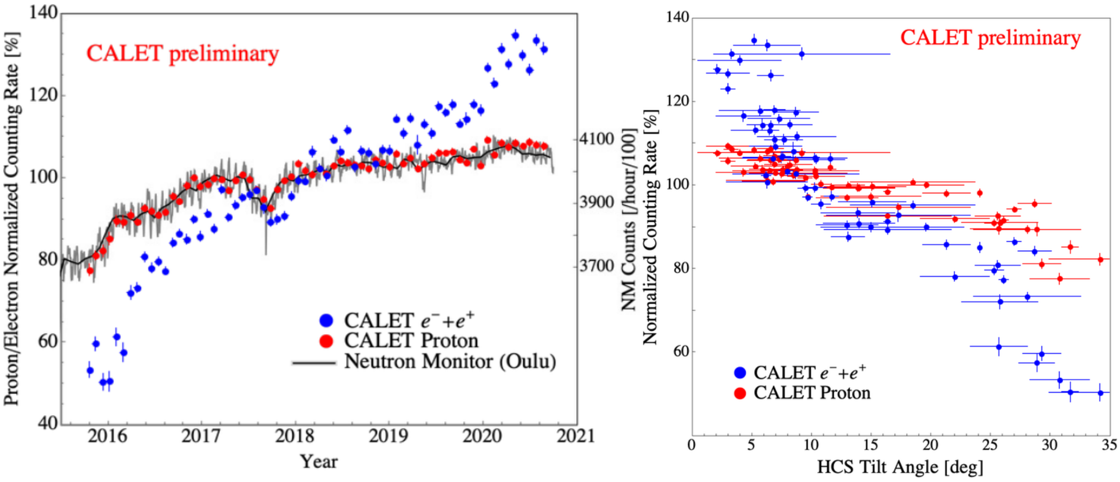

Figure 4: (Left panel) Time profiles of normalized count rates of electrons and protons from October 2015 to September 2020 for each Carrington rotation. Count rates of electrons and protons are normalized with each first count rate. (Right panel) Correlation with normalized count rates of electrons and protons and a tilt angle of the heliospheric current sheet.

5. Charge Sign Dependence of the Solar Modulation

In order to investigate the charge sign dependence of the solar modulation, we have also evaluated the count rate of electrons and protons that have an average rigidity of ~ 3.8 GV. Left panel of Figure 4 shows the time profile of count rates of the electrons (blue markers) and protons (red markers) observed by CALET. In this figure, the average count rate over a period between October 13, 2015 and September 30, 2020 is normalized to 100. A count rate of a neutron monitor at Oulu Station (a Black line with a gray line) is also shown for a comparison with a normalized proton count rate. We can find that the proton count rate also increases with decreasing the solar activity in a manner very similar to that of the neutron monitor count rate. We actually obtained a strong correlation between proton and neutron monitor count rates with a correlation coefficient of 0.97. This verifies the validity of our derivation of proton count rate. What is interesting here is that the observed variation amplitude of electron count rate is clearly larger than that of proton count rate. This charge-sign dependence of the modulation is expected from the so-called drift model predicting that CRs propagate along the different paths depending on the heliospheric magnetic polarity A and the CR's charge q. Particles propagate from the polar region of the heliosphere toward the Earth due to the drift motion in case of $qA>0$, whereas they propagate along the heliospheric current sheet (HCS) from the outer heliosphere in case of $qA<0$. Because the current solar cycle is the $A > 0$ epoch, the charge sign qA for the electron is Negative. Therefore the flux of electrons is expected to change larger than that of protons according to the solar-cycle variation of the HCS tilt angle. Our results of electron and proton count rates in the right panel of Figure 4 show the charge sign dependence that is consistent at least qualitatively with the drift model prediction of the solar modulation.

PoS(ICRC2021)1270

6. Conclusion

We have analyzed the flux of low-energy electrons and protons measured by CALET from October 2015 to September 2020, and have successfully obtained count rates of electrons and protons that have the same average rigidity. We have confirmed that the flux of the low-energy electrons measured by CALET during the solar minimum has reached its maximum, which is comparable to or exceeding the maximum flux observed with PAMELA in previous solar minimum period. We have also found the modulation amplitude of electron count rate is clearly larger than that of proton count rate. There is consistent with the charge sign dependence expected from the drift model of the solar modulation.

Acknowledgments

We thank Ilya Usoskin from Sodankyla Geophysical Observatory of the University of Oulu to provide Oulu neutron monitor data online. This work is partially supported by JSPS KAKENHI grant JP20K03956.

References

[1] O. Adriani et al. (CALET Collaboration), Phys. Rev. Lett., **119**, 181101 (2017)

[2] O. Adriani et al. (CALET Collaboration), Phys. Rev. Lett., **120**, 261102 (2018)

[3] O. Adriani et al. (CALET Collaboration), Phys. Rev. Lett. **122**, 181102 (2019)

[4] O. Adriani et al. (CALET Collaboration), Phys. Rev. Lett. **125**, 251102 (2020)

[5] Y. Asaoka, Y. Akaike, Y. Komiya, R. Miyata, S. Torii et al. (CALET Collaboration), Astropart. Phys. **91**, 1 (2017)

[6] Y. Asaoka, Y. Ozawa, S. Torii et al. (CALET Collaboration), Astropart. Phys. **100**, 29 (2018)

[7] K. Kasahara, in *Proceeding of the 24th International Cosmic Ray Conference, Rome, Italy*, **1**, 399 (1995)

[8] S. Miyake, R. Kataoka, and T. Sato, Space Weather, **15**, 4, 589-605 (2017)

[9] N. A. Tsyganenko, Journal of Geophysical Research, **110**, A03208 (2005)

[10] O. Adriani et al. (PAMELA Collaboration), Astrophys. J., **810**, 142 (2015)

PoS(ICRC2021)1270

Full Authors List: CALET Collaboration

O. Adriani[1,2], Y. Akaike[3,4], K. Asano[5], Y. Asaoka[5], E. Berti[1,2], G. Bigongiari[6,7], W. R. Binns[8], M. Bongi[1,2], P. Brogi[6,7], A. Bruno[9,10], J. H. Buckley[8], N. Cannady[11,12,13], G. Castellini[14], C. Checchia[6], M. L. Cherry[15], G. Collazuol[16,17], K. Ebisawa[18], A. W. Ficklin[15], H. Fuke[18], S. Gonzi[1,2], T. G. Guzik[15], T. Hams[11], K. Hibino[19], M. Ichimura[20], K. Ioka[21], W. Ishizaki[5], M. H. Israel[8], K. Kasahara[22], J. Kataoka[23], R. Kataoka[24], Y. Katayose[25], C. Kato[26], N. Kawanaka[27,28], Y. Kawakubo[15], K. Kobayashi[3,4], K. Kohri[29], H. S. Krawczynski[8], J. F. Krizmanic[11,12,13], P. Maestro[6,7], P. S. Marrocchesi[6,7], A. M. Messineo[30,7], J.W. Mitchell[12], S. Miyake[32], A. A. Moiseev[33,12,13], M. Mori[34], N. Mori[2], H. M. Motz[35], K. Munakata[26], S. Nakahira[18], J. Nishimura[18], G. A. de Nolfo[9], S. Okuno[19], J. F. Ormes[36], N. Ospina[16,17], S. Ozawa[37], L. Pacini[1,14,2], P. Papini[2], B. F. Rauch[8], S. B. Ricciarini[14,2], K. Sakai[11,12,13], T. Sakamoto[38], M. Sasaki[33,12,13], Y. Shimizu[19], A. Shiomi[39], P. Spillantini[1], F. Stolzi[6,7], S. Sugita[38], A. Sulaj[6,7], M. Takita[5], T. Tamura[19], T. Terasawa[40], S. Torii[3], Y. Tsunesada[41], Y. Uchihori[42], E. Vannuccini[2], J. P. Wefel[15], K. Yamaoka[43], S. Yanagita[44], A. Yoshida[38], K. Yoshida[22], and W. V. Zober[8]

[1]Department of Physics, University of Florence, Via Sansone, 1, 50019 Sesto, Fiorentino, Italy, [2]INFN Sezione di Florence, Via Sansone, 1, 50019 Sesto, Fiorentino, Italy, [3]Waseda Research Institute for Science and Engineering, Waseda University, 17 Kikuicho, Shinjuku, Tokyo 162-0044, Japan, [4]JEM Utilization Center, Human Spaceflight Technology Directorate, Japan Aerospace Exploration Agency, 2-1-1 Sengen, Tsukuba, Ibaraki 305-8505, Japan, [5]Institute for Cosmic Ray Research, The University of Tokyo, 5-1-5 Kashiwa-no-Ha, Kashiwa, Chiba 277-8582, Japan, [6]Department of Physical Sciences, Earth and Environment, University of Siena, via Roma 56, 53100 Siena, Italy, [7]INFN Sezione di Pisa, Polo Fibonacci, Largo B. Pontecorvo, 3, 56127 Pisa, Italy, [8]Department of Physics and McDonnell Center for the Space Sciences, Washington University, One Brookings Drive, St. Louis, Missouri 63130-4899, USA, [9]Heliospheric Physics Laboratory, NASA/GSFC, Greenbelt, Maryland 20771, USA, [10]Department of Physics, Catholic University of America, Washington, DC 20064, USA, [11]Center for Space Sciences and Technology, University of Maryland, Baltimore County, 1000 Hilltop Circle, Baltimore, Maryland 21250, USA, [12]Astroparticle Physics Laboratory, NASA/GSFC, Greenbelt, Maryland 20771, USA, [13]Center for Research and Exploration in Space Sciences and Technology, NASA/GSFC, Greenbelt, Maryland 20771, USA, [14]Institute of Applied Physics (IFAC), National Research Council (CNR), Via Madonna del Piano, 10, 50019 Sesto, Fiorentino, Italy, [15]Department of Physics and Astronomy, Louisiana State University, 202 Nicholson Hall, Baton Rouge, Louisiana 70803, USA, [16]Department of Physics and Astronomy, University of Padova, Via Marzolo, 8, 35131 Padova, Italy, [17]INFN Sezione di Padova, Via Marzolo, 8, 35131 Padova, Italy, [18]Institute of Space and Astronautical Science, Japan Aerospace Exploration Agency, 3-1-1 Yoshinodai, Chuo, Sagamihara, Kanagawa 252-5210, Japan, [19]Kanagawa University, 3-27-1 Rokkakubashi, Kanagawa, Yokohama, Kanagawa 221-8686, Japan, [20]Faculty of Science and Technology, Graduate School of Science and Technology,, Hirosaki University, 3, Bunkyo, Hirosaki, Aomori 036-8561, Japan, [21]Yukawa Institute for Theoretical Physics, Kyoto University, Kitashirakawa Oiwakecho, Sakyo, Kyoto 606-8502, Japan, [22]Department of Electronic Information Systems, Shibaura Institute of Technology, 307 Fukasaku, Minuma, Saitama 337-8570, Japan, [23]School of Advanced Science and Engineering, Waseda University, 3-4-1 Okubo, Shinjuku, Tokyo 169-8555, Japan, [24]National Institute of Polar Research, 10-3, Midori-cho, Tachikawa, Tokyo 190-8518, Japan, [25]Faculty of Engineering, Division of Intelligent Systems Engineering, Yokohama National University, 79-5 Tokiwadai, Hodogaya, Yokohama 240-8501, Japan, [26]Faculty of Science, Shinshu University, 3-1-1 Asahi, Matsumoto, Nagano 390-8621, Japan, [27]Hakubi Center, Kyoto University, Yoshida Honmachi, Sakyo-ku, Kyoto 606-8501, Japan, [28]Department of Astronomy, Graduate School of Science, Kyoto University, Kitashirakawa Oiwake-cho, Sakyo-ku, Kyoto 606-8502, Japan, [29]Institute of Particle and Nuclear Studies, High Energy Accelerator Research Organization, 1-1 Oho, Tsukuba, Ibaraki 305-0801, Japan, [30]University of Pisa, Polo Fibonacci, Largo B. Pontecorvo, 3, 56127 Pisa, Italy, [31]Astroparticle Physics Laboratory, NASA/GSFC, Greenbelt, Maryland 20771, USA, [32]Department of Electrical and Electronic Systems Engineering, National Institute of Technology, Ibaraki College, 866 Nakane, Hitachinaka, Ibaraki 312-8508, Japan [33]Department of Astronomy, University of Maryland, College Park, Maryland 20742, USA, [34]Department of Physical Sciences, College of Science and Engineering, Ritsumeikan University, Shiga 525-8577, Japan, [35]Faculty of Science and Engineering, Global Center for Science and Engineering, Waseda University, 3-4-1 Okubo, Shinjuku, Tokyo 169-8555, Japan, [36]Department of Physics and Astronomy, University of Denver, Physics Building, Room 211, 2112 East Wesley Avenue, Denver, Colorado 80208-6900, USA, [37]Quantum ICT Advanced Development Center, National Institute of Information and Communications Technology, 4-2-1 Nukui-Kitamachi, Koganei, Tokyo 184-8795, Japan, [38]College of Science and Engineering, Department of Physics and Mathematics, Aoyama Gakuin University, 5-10-1 Fuchinobe, Chuo, Sagamihara, Kanagawa 252-5258, Japan, [39]College of Industrial Technology, Nihon University, 1-2-1 Izumi, Narashino, Chiba 275-8575, Japan [40]RIKEN, 2-1 Hirosawa, Wako, Saitama 351-0198, Japan, [41]Division of Mathematics and Physics, Graduate School of Science, Osaka City University, 3-3-138 Sugimoto, Sumiyoshi, Osaka 558-8585, Japan, [42]National Institutes for Quantum and Radiation Science and Technology, 4-9-1 Anagawa, Inage, Chiba 263-8555, Japan, [43]Nagoya University, Furo, Chikusa, Nagoya 464-8601, Japan, [44]College of Science, Ibaraki University, 2-1-1 Bunkyo, Mito, Ibaraki 310-8512, Japan

PoS(ICRC2021)1270